

# Deep Learning Using High-Resolution Images of Forearm Predicts Fracture

**Running head:** Fracture Prediction using Deep Learning

Roland Chapurlat<sup>1</sup>

Serge Ferrari<sup>2</sup>

Xiaoxu Li<sup>3</sup>

Yu Peng<sup>3</sup>

Min Xu<sup>4</sup>

Min Bui<sup>5</sup>

Elisabeth Sornay-Rendu<sup>1</sup>

Eric lespessailles<sup>6</sup>

Emmanuel Biver<sup>2</sup>

Ego Seeman<sup>7</sup>

<sup>1</sup>INSERM UMR 1033, Université Claude Bernard-Lyon1, Hospices Civils de Lyon, Lyon, France

<sup>2</sup>University of Geneva, Geneva, Switzerland

<sup>3</sup>CurvebeamAI, Melbourne

<sup>4</sup>University of Technology Sydney

<sup>5</sup>Centre for Epidemiology and Biostatistics, School of Population and Global Health, University of Melbourne, Melbourne, Australia

<sup>6</sup>IPROS, CHR d'Orléans

<sup>7</sup>Depts Endocrinology and Medicine, Austin Health, University of Melbourne<sup>1</sup>

Correspondence: Roland Chapurlat

53

## Key Points

54

55 **Question** Can a deep learning model (DL)<sup>o</sup> based on high resolution images of the distal  
56 forearm predict fragility fractures?

57

58 **Findings** In the setting of 3 pooled population-based cohorts, the DL model predicted  
59 fractures substantially better than areal bone mineral density and FRAX, especially in women  
60  $\geq 65$  years.

61

62 **Meaning** Our DL model may become an easy to use way to identify postmenopausal women  
63 at risk for fracture to improve fracture prevention.

64

65

66

67

## Abstract

68

69 **Importance** Fragility fractures are a public health problem. Over 70% of women having  
70 fractures have osteopenia or normal BMD, but they remain unidentified and untreated  
71 because the definition of ‘osteoporosis’, a bone mineral density (BMD) T-Score  $\leq -2.5SD$ , is  
72 often used to signal bone fragility.

73

74 **Objective** As deep learning facilitates investigation of bone’s multi-level hierarchical  
75 structure and soft tissue, we tested whether this approach might better identify women at risk  
76 of fracture before fracture.

77

78 **Design** We pooled data from three French and Swiss prospective population-based cohorts  
79 (OFELY, QUALYOR, GERICO) that collected clinical risk factors for fracture, areal BMD  
80 and distal radius measurements with high resolution peripheral quantitative tomography  
81 (HRpQCT). Using only three-dimensional images of the distal radius, ulna and soft tissue  
82 acquired by HRpQCT, an algorithm, a Structural Fragility Score-Artificial Intelligence (SFS-

83 AI), was trained to distinguish 277 women having fractures from 1401 remaining fracture-free  
84 during 5 years and then was tested in a validation cohort of 422 women.

85

86 **Setting** European postmenopausal women

87

88 **Participants** We have studied postmenopausal women considered as representative of the  
89 general population, who were followed for a median 9.4 years in OFELY, 5.4 years in  
90 QUALYOR and 5.7 years in GERICO.

91

92 **Main outcome and measure** All types of incident fragility fractures

93

94 **Results** We used data from 2666 postmenopausal women, with age range of 42-94. In women  
95  $\geq 65$  years having ‘All Fragility Fractures’ or ‘Major Fragility Fractures’, SFS-AI generated  
96 an AUC of 66-70%, sensitivities of 60-68% and specificity of 71%. Sensitivities were greater  
97 than achieved by the fracture risk assessment (FRAX) with BMD or BMD (6.7-26.7%) with  
98 lower specificities than these diagnostics (~95%).

99

100 **Conclusion and relevance** The SFS-AI is a holistic surrogate of fracture risk that pre-  
101 emptively identifies most women needing prompt treatment to avert a first fracture.

102

103

104 **Key words:** Artificial Intelligence, Bone Structure, Bone Fragility, Deep Learning, Fractures

105

106

107

108

109 **Introduction**

110

111 Fragility fractures are a public health problem because fractures impose high morbidity,  
112 mortality and cost to the community.<sup>1</sup> To identify women with fragile bones before fracture, a  
113 W.H.O group designated women as having ‘osteoporosis’ if femoral neck bone mineral  
114 density (BMD) T-Score was  $\leq -2.5$  standardized deviations (SD) below the premenopausal  
115 mean.<sup>2</sup> Epidemiological studies confirmed that fracture risk increases as BMD decreases, but  
116 the frequency distribution around the age-related decline in mean BMD remains normal.

117

118 Because of this normal frequency distribution, most postmenopausal women in the  
119 community have osteopenia (T-score  $-2.5$  to  $-1.0$  SD) or normal BMD (T-score  $> -1.0$  SD).  
120 These women form the source of 75% of all fragility in the community, only 25% arise  
121 among the smaller subset of women in the community with osteoporosis as defined by  
122 BMD.<sup>3-9</sup> The women with osteopenia or normal BMD having fragility fractures remain  
123 unidentified and untreated using the definition of osteoporosis, a BMD T-Score  $\leq -2.5$  SD, to  
124 signal bone fragility. Treatment is not offered, even in the presence of a prevalent or incident  
125 fracture, because the absence of osteoporosis is incorrectly interpreted as being evidence of  
126 absence of bone fragility.<sup>10</sup>

127

128 Osteoporosis and bone fragility are used interchangeably even though they are not  
129 synonymous terms.<sup>11-13</sup> Absence of osteoporosis does not exclude bone fragility. Bone  
130 fragility is not binary, present in women with osteoporosis (T-Score  $\leq -2.5$  SD) and absent in  
131 women without osteoporosis (T-Score  $> -2.5$  SD). Even when bone loss only reduces BMD  
132 into the low normal or osteopenia range, the bone is unlikely to be ‘normal’. Bone mass is  
133 reduced relative to premenopausal women and many qualities of bone responsible for its  
134 strength may be compromised.<sup>14-18</sup>

135

136 For example, advancing age deteriorates the composition of the mineralized matrix.<sup>19,20</sup> Bone  
137 loss disrupts the spatial configuration of bone's three-dimensional architecture.<sup>15,21</sup> These  
138 changes produce a non-linear increase in bone fragility, disproportionate to both the bone loss  
139 causing the deterioration and the reduction in BMD.<sup>20,22</sup> Resistance to bending is a 7<sup>th</sup> power  
140 function of bone's cortical porosity and a 3<sup>rd</sup> power function of its trabecular density.<sup>22</sup>

141

142 Consequently, even modest disruption of the spatial configuration of bone at nano-, and  
143 micro-levels of resolution compromise bone strength independent of BMD. In addition, soft  
144 tissue changes like loss of muscle mass (sarcopenia) impair mobility and balance predisposing  
145 to falls, fractures and mortality.<sup>23</sup> Thus, reducing the population burden of fractures requires a  
146 diagnostic that complements BMD by identifying women at risk of fracture due to bone  
147 fragility caused by compromised bone morphology not captured by  $BMD \leq -2.5$  SD, by an  
148 increased risk of falls due to deteriorated soft tissues such as muscle mass, or both. Non-  
149 invasive evaluation of bone microarchitecture improves fracture prediction compared with  
150 FRAX plus BMD or BMD alone.<sup>8,9</sup>

151

152 A promising area of innovation in the promotion of human health is the use of Artificial  
153 Intelligence (AI). Application of Deep Learning to medical imaging<sup>24</sup> facilitates the  
154 investigation of bone's multilayered qualities and has been reported to identify patients with  
155 prevalent fractures or osteoporosis in cross sectional studies.<sup>25-27</sup> However, no prospective  
156 studies have applied deep learning using only the high resolution 3-dimensional images of  
157 bone and soft tissue to determine whether an algorithm, a Structural Fragility Score derived  
158 by Artificial Intelligence (SFS-AI), might capture deteriorated bone qualities and soft tissue.  
159 If so, this holistic surrogate of fracture risk is likely to serve as a diagnostic that pre-emptively

160 identifies women at risk of a first or subsequent fracture needing prompt treatment and would  
161 do so better than the fracture risk assessment (FRAX) score with BMD or BMD alone.

162

163

164

165

166

167

168

169

170

171

172

173

174

175

176

177

178

179

180

181

182

183

184

185

186 **Methods**

187

188 **Participants** We studied (i) 568 postmenopausal women, median age 68.2 years, range 42-  
189 94 of Os des Femmes de LYon, OFELY, France followed for a median [interquartile range]  
190 of 9.4 [1.0] years,<sup>9,28,29</sup> (ii) 1427 women of the Qualité Osseuse Lyon Orléans, QUALYOR  
191 cohort (1042 recruited in Lyon, 497 in Orléans), median age 65.9 (range 50-87) years  
192 followed for 5 years<sup>30</sup> and (iii) 671 women of the Geneva Retirees Cohort, GERICO, in  
193 Switzerland median age 65 (range 63-68) years followed 5.7 years (range 2-8).<sup>31</sup> The studies  
194 were approved by the institutional review boards. Participants provided informed consent.  
195 Fractures (excluding head, toes and fingers) were confirmed using radiographs.

196

197 **Bone microarchitecture, bone densitometry, FRAX with BMD** HRpQCT (voxel size of  
198 82  $\mu\text{m}^3$ ) was used to scan the non-dominant forearm (Scanco Medical AG, Switzerland).<sup>32</sup>  
199 Radiation exposure was ~3 microsievert. Quality control was monitored by daily scans of  
200 hydroxyapatite rods (QRM, Moehrendorf, Germany). Femoral neck BMD was quantified  
201 using Hologic DXA scanners in the French cohorts and Hologic QDR Discovery in the Swiss  
202 cohort. T-scores were calculated using NHANES III. FRAX with femoral neck BMD  
203 provides a 10-year risk for Major Fragility Fractures (proximal humerus, wrist, distal forearm,  
204 clinical spine, or hip).<sup>33</sup>

205

206 **Deep Learning network** To avoid bias towards any one of the three cohorts, we  
207 combined the three cohorts and then we randomly divided the combined data set into a  
208 training and testing data set. No training data was used as testing data. **Figure S2** shows  
209 participants were randomly allocated to five groups, four used for training (n=1678), the fifth  
210 used for testing (n = 422). Scores were calculated for each testing group with the median  
211 forming the SFS-AI (see Supplement **Figure S2**). Deep learning was applied to images of the

212 distal radius and ulna and the surrounding soft tissue acquired using HR-pQCT (see  
213 Supplement).<sup>34-37</sup> Training the algorithm to identify women sustaining fractures faced two  
214 challenges: (i) extraction of features within the three-dimensional image captured by a matrix  
215 of 110\*1560\*1560 voxels conferring fracture risk and (ii) limited data for training  
216 predisposing to model over-fitting. We used the DenseNet121 as the feature extraction  
217 network (**Figure S1**). Features conferring fracture risk were learnt collectively by densely  
218 connected layers in the neural network. The input to the feature extraction network was the  
219 110 slices acquired by the HR-pQCT at the distal radius (including the ulna and surrounding  
220 soft tissues). The output from the feature extraction network is a feature vector of 256  
221 numbers.

222

223 To achieve robust feature extraction, a multi-task learning strategy was used to overcome  
224 model overfitting. To provide pictorial representation of the fracture risk prediction, extracted  
225 features were displayed as a heat map overlaid upon a 2D projection of the images. Red  
226 reflects greater relevance of the region's bone or soft tissue to fracture prediction.

227

228 **Statistical Analyses** Analyses were conducted using data in women of any age and those 65  
229 years and over. Follow-up was to fracture or freedom from fracture for five years since HR-  
230 pQCT scanning. SFS-AI, FRAX with BMD and BMD were not normally distributed and so  
231 are presented as median and interquartile range (IQR). Values are adjusted for age and cohort  
232 because of cohort differences in age and follow-up duration. (**Tables S1 and S2.**) Comparison  
233 of the diagnostics in women having fractures and those remaining fracture-free was carried  
234 out using analysis of covariance adjusted for age and cohort and estimated by robust  
235 regression. (**Table 1.**)

236



237 The performance of SFS-AI as a continuous trait was assessed using the area under the curve  
238 (AUC) and was estimated using a parametric probit model<sup>38</sup> and logistic regression to derive  
239 Odds Ratios (ORs) for fracture. Both analyses are presented unadjusted and adjusted for age  
240 and cohort effect. The sensitivity and specificity of SFS-AI as a binary trait used a threshold  
241 of 0.5. (Addressed in **Table 2.**)

242

243 We also assessed the performance of FRAX with BMD and BMD as continuous traits using  
244 ROC analysis and computed sensitivity and specificity using thresholds of 20% for FRAX  
245 with BMD and – 2.5 SD for BMD denoting high fracture risk. Logistic regression was then  
246 used to assess any association of these diagnostics with fracture, separately and combined, for  
247 women of any age and women aged 65 years and over. (Addressed in **Figure 1 and Table**  
248 **S3.**)

249

250 Linear regression was used to assess the association of SFS-AI with age, separately for  
251 women with fractures and women remaining fracture-free. (Addressed in **Figure 2.**) Age,  
252 cortical porosity, trabecular density, FRAX with BMD and BMD were used in linear  
253 regression to compute an overall R-squared and to determine the proportion of variance in  
254 SFS-AI explained by these independent variables. The percentage contribution of each trait  
255 to the overall R-squared was computed using the Shapley method.<sup>39</sup> (Addressed in **Table S5**  
256 **and Figure 3.**)

257

258

259

260

261

262

263 **Results**

264

265 **Table 1** shows SFS-AI was higher in women having ‘All’ or ‘Major Fragility Fractures’ than  
266 women remaining fracture-free (both  $p < 0.001$ ). Neither FRAX with BMD nor BMD alone  
267 differed in women having fractures versus those remaining fracture-free ( $p > 0.15$ ).

268

269 **SFS-AI pre-emptively identifies women at risk of ‘All’ and ‘Major Fragility Fractures’**

270

271 **Table 2** shows that in the testing cohort of 422 women of any age and the 236 women  $\geq 65$   
272 years of age, the SFS-AI as a continuous trait generated AUCs of 73-74% for ‘All Fragility  
273 Fractures’ and ‘Major Fragility fractures’ with adjusted ORs ranging from 2.53 to 2.67 per  
274 standard deviation. The SFS-AI as a categorical trait (using a threshold of 0.5), had  
275 sensitivities ranging from 58.1% to 74.0% and specificities ranging from 71.0% to 77.3% (all  
276 significant,  $p < 0.001$  for OR and AUC).

277

278 **Comparing SFS-AI with FRAX with BMD and BMD**

279

280 **Women of any age** Comparisons of the diagnostics was confined to participants having all  
281 three measurements. **Figure 1** shows the diagnostics as continuous traits. For ‘All Fragility  
282 Fractures’ and ‘Major Fragility Fractures’, the AUCs for SFS-AI were 72% and 69%  
283 respectively ( $p < 0.05$ ). **Table S3** shows unadjusted and adjusted SFS-AI predicted women  
284 having either category of fractures (ORs ranged from 2.07 to 2.41, all  $p < 0.001$ ). Neither of  
285 the other two diagnostics predicted either category of fracture. **Figure 1** also shows the  
286 diagnostics as categorical traits. For SFS-AI, sensitivities were 59.3% and 50.0% for  
287 detecting women having ‘All Fragility Fractures’ or ‘Major Fragility Fractures’ respectively,  
288 values that were significantly greater than sensitivities of FRAX with BMD or BMD (which

289 ranged 4.2 to 16.7%). Specificities of SFS-AI were 77.1%, significantly lower than  
290 specificities of the other two diagnostics (which ranged 94.6 to 96.6%).

291

292 **Women aged  $\geq 65$  years** Supplementary **Figure S3** shows the performance of the  
293 diagnostics as continuous traits. For ‘All Fragility Fractures’ and ‘Major Fragility Fractures’,  
294 the AUCs for SFS-AI were 70% and 66% respectively. **Table S4** shows unadjusted and  
295 adjusted SFS-AI predicted both categories of fractures (OR 1.68 to 2.15, all  $p < 0.05$ ).  
296 Neither of the other two diagnostics predicted either category of fracture. **Figure S3** also  
297 shows the performance of the diagnostics as categorical traits. For SFS-AI, sensitivities were  
298 67.6% and 60.0% for detecting women having ‘All Fragility Fractures’ or ‘Major Fragility  
299 Fractures’ respectively, values significantly greater than the sensitivities of FRAX with BMD  
300 or BMD (ranging 6.67 to 26.7%). Specificities of SFS-AI were 70.7%, significantly lower  
301 than specificity of 94.6% for the other two diagnostics.

302

303 **The morphological basis of the SFS-AI** **Figure 2** shows that SFS-AI increased across  
304 age in women having fragility fractures and in women remaining fracture-free. Red regions  
305 of the heat map overlying bone and soft tissue identify regions of high relevance to risk of  
306 incident fractures compared to the blue regions. **Figure 3** shows that SFS-AI correlated with  
307 microarchitecture; directly with cortical porosity and FRAX with BMD, and negatively with  
308 trabecular density and BMD. **Figure 3** and Supplementary **Table S5** show that 46% of the  
309 variance in SFS-AI was explained by variance in age ( $p = 0.002$ ), cortical porosity and  
310 trabecular density (both  $p < 0.001$ ) but not with BMD or FRAX with BMD; 54% of the  
311 variance remained unexplained.

312

313

314

315 **Discussion**

316

317 A deep learning algorithm was trained to identify women having fragility fractures using only  
318 the high-resolution three-dimensional images of bone and soft tissue. No other information  
319 was used. When training no longer improved predictive strength, the algorithm was tested in  
320 a cohort without knowledge of their fracture status during the ensuing 5 years. This algorithm  
321 served as a surrogate of fracture risk, predicting the incidence of ‘All Fragility Fractures’ and  
322 ‘Major Fragility Fractures’ and did so in women 65 years and older with a sensitivity and  
323 specificity of 60-70%, out-performing BMD and FRAX with BMD, neither of which  
324 predicted fractures.

325

326 This surrogate of fracture risk, a Structural Fragility Score derived by deep learning artificial  
327 intelligence, increased across advancing age, was higher in women having incident fractures  
328 than those remaining fracture-free, and correlated directly with cortical porosity and  
329 negatively with trabecular density. Deterioration of these two traits produces a nonlinear  
330 increase in bone fragility,<sup>22</sup> predicts incident fractures,<sup>8,9</sup> prevalent fractures<sup>40</sup> and predicts  
331 estimated bone strength independent of BMD.<sup>41</sup> Deterioration of these two traits accounted  
332 for most of the 48% explained variance in SFS-AI. BMD was not an independent predictor of  
333 SFS-AI.

334

335 Many qualities of bone not captured by BMD but not yet quantifiable non-invasively, may  
336 contribute to the 54% of the unexplained variance in this surrogate of fracture risk.<sup>14-19</sup> For  
337 example, heterogeneity in bone’s material composition forms discontinuities, edges, that  
338 defend against fracture by increasing the energy required to initiate and propagate a crack.<sup>42</sup>  
339 Small changes in the degree of mineralization increase matrix stiffness but reduce its ductility  
340 (ability to absorb energy by deforming).<sup>43</sup> Heterogeneity in the size and number of osteons,<sup>44</sup>

341 the cement line around each osteon,<sup>45,46</sup> the differing orientation of mineralized collagen  
342 fibres of adjacent concentric osteonal lamellae,<sup>47-49</sup> the extent glycation,<sup>50</sup> hydration<sup>51</sup> and  
343 other factors<sup>52,53</sup> influence the mechanical properties of bone. The heat map implicated  
344 deterioration of soft tissue as well as bone. The nature of soft tissue deterioration is not  
345 known but if it is sarcopenia then the SFS-AI algorithm might capture a component of risk for  
346 falls.<sup>23</sup>

347

348 Most studies using machine learning are cross sectional and examine the ability to identify  
349 persons with prevalent fractures or osteoporosis (BMD T-Score  $\leq$  - 2.5 SD).<sup>24-27</sup> This is the  
350 first prospective study using deep learning to derive an algorithm that identifies women  
351 having incident fractures during five years. The algorithm was developed by interrogating the  
352 three-dimensional images of bone and soft tissue, no other information was used. This  
353 Structural Fragility Score serves as a surrogate of fracture risk that is likely to assist in  
354 reducing the population burden of fragility fractures. It provides a diagnostic able to identify  
355 most women at risk of fracture and provides fast processing, easy access to risk assessment  
356 allowing prompt initiation and monitoring of preventative treatment at the community level.

357

358 High resolution peripheral quantitative computed tomography (HRpQCT) technology is no-  
359 longer confined to the research domain. Commercial devices are now CE marked and FDA  
360 cleared for multiple clinical settings. Analysis requires only the acquisition of the three-  
361 dimensional image of the distal radius, ulna and soft tissue and cloud-based computer  
362 technology provides prompt diagnosis allowing initiation or monitoring of therapy.

363

364 This study has several limitations. Further studies are needed to determine whether including  
365 factors predisposing to falls such as muscle mass and function, age, height, weight and other

366 covariates improves the performance of the diagnostic. The sample sizes were insufficient to  
367 evaluate performance of the diagnostic in predicting individual types of fracture.

368

369 Advancing age is accompanied by deterioration in bone mass, its material composition,  
370 architecture and muscle mass - factors contributing to fragility fractures, a public health  
371 problem. High-resolution quantitative computed tomography and deep learning provide a  
372 Structural Fragility Score that serves as a holistic surrogate of fracture risk. This diagnostic is  
373 an accurate, safe, rapid and easily accessible tool that captures the deterioration of bone  
374 qualities contributing to bone fragility independent of BMD and perhaps deterioration of  
375 muscle predisposing falls. This surrogate identifies women at high risk of fracture needing  
376 prompt treatment to avert fracture and may allow monitoring the success or failure of  
377 treatment.

378

379

380

381

382

383

384

385

386

387

388

389

390

391

392 **Legends for Figures for manuscript**

393

394 **Figure 1. Left two panels:** Receiver Operator Characteristic (ROC) curves for Structural  
395 Fragility Score Artificial Intelligence (SFS-AI), Fracture Risk Assessment Score (FRAX) with  
396 bone mineral density (BMD) and BMD as a continuous trait predicting for ‘All Fragility  
397 Fractures’ and ‘Majority Fragility Fractures’ for women of any age. Area under the Curves  
398 (AUCs) with 95% Confidence Intervals (CI) were significant ( $*p < 0.05$ ) for SFS-AI only.

399 **Right two panels:** Sensitivity and specificity of SFS-AI, FRAX with BMD and BMD as  
400 categorical traits.

401

402 **Figure 2. Left panels:** Advancing age is associated with a higher Structural Fragility Score-  
403 Artificial Intelligence (SFS-AI) in women having ‘All Fragility Fractures’ or Major Fragility  
404 Fractures (closed circles) and in women remaining fracture-free (open circles). The images of  
405 the distal radius and ulna with the heat map illustrate regions commonly encountered in  
406 women having fractures.

407

408 **Figure 3. Left panels.** The Structural Fragility Score-Artificial Intelligence (SFS-AI) was  
409 associated directly with cortical porosity, FRAX with BMD and negatively with trabecular  
410 density and BMD. **Right diagram.** Of the 47% of explained variance in the SFS-AI, most  
411 was attributed to trabecular density, cortical porosity, age and the FRAX with BMD. The  
412 contribution of BMD was not significant. The remaining 53 percent remained unexplained.

413

414 **Legends for Figures in supplementary material**

415

416 **Figure S1.** Structure of the deep learning model used to predict fracture. The input is the 110  
417 slices of a wrist scan used to acquire the three-dimensional image of the distal radius, distal

418 ulna and adjacent soft tissue. DenseNet121 is used as the neural network backbone. The  
419 output feature after the global average pool is a 256-dimension feature. A multi-task (age  
420 prediction, fracture prediction and non-fracture years prediction) learning strategy was used to  
421 achieve robust extraction of relevant features.

422

423 **Figure S2.** We studied women from OFELY (n = 568), Qalyor (n = 1427) and Gerico (n =  
424 671). (A) There were 526, 1187 and 387 images remaining from the respective cohorts for  
425 analysis after excluding images from women remaining fracture-free followed for under 5  
426 years and images from women having traumatic (non-fragility). (B) Women having a  
427 fragility fracture during 5 years were denoted as (+), women remaining fracture-free as (-).  
428 (C) Participants from each cohort were randomly allotted into five groups with approximately  
429 equal numbers of (+) and (-) subjects. See Methods section.

430

431 **Figure S3. Left two panels.** Receiver Operator Characteristic (ROC) curves for Structural  
432 Fragility Score Artificial Intelligence (SFS-AI), Fracture Risk Assessment Score (FRAX) with  
433 bone mineral density (BMD) and BMD as continuous traits predicting ‘All Fragility  
434 Fractures’ and ‘Major Fragility Fractures’ in women 65 years of age and over. Area under the  
435 Curves (AUCs) with 95% Confidence Intervals (CI) were significantly different from 0.5 (\*p  
436 < 0.05) for SFS-AI only. **Right two panels.** Sensitivity and specificity of the SFS-AI, FRAX  
437 with BMD and BMD as categorical traits predicting women having ‘All Fragility Fractures’  
438 or ‘Major Fragility Fractures’.

439

440

441

442

443

444



445 **References**

446

447. Compston JE, McClung M, Leslie W. Osteoporosis. *Lancet* 2019;393: 364-76

448. Kanis JA. Assessment of fracture risk and its application to screening for postmenopausal

449 osteoporosis: synopsis of a WHO report. WHO Study Group. *Osteoporos Int.* 1994;4: 368–81.

450. Siris ES, Chen YT, Abbott TA, et al. Bone mineral density thresholds for pharmacological

451 intervention to prevent fractures. *Arch Intern Med.* 2004;164: 1108–12.

452. Schuit SC, van der Klift M, Weel AE, et al. Fracture incidence and association with bone

453 mineral density in elderly men and women: the Rotterdam Study. *Bone.* 2004;34:195–202.

454. Pasco JA, Seeman E, Henry MJ, et al. The population burden of fractures originates in women

455 with osteopenia, not osteoporosis. *Osteoporos Int.* 2006;17:1404–9.

456. Sanders KM, Nicholson GC, Watts JJ, et al. Half the burden of fragility fractures in the

457 community occur in women without osteoporosis. When is fracture prevention cost-effective?

458 *Bone.* 2006;38: 694–700.

459. Trajanoska K, Schoufour JD, de Jonge EAL et al. Fracture incidence and secular trends

460 between 1989 and 2013 in a population-based cohort: The Rotterdam Study *Bone.*

461 2018;114:116–24.

462. Samelson EJ, Broe KE, Xu H et al. Cortical and trabecular bone microarchitecture as an

463 independent predictor of incident fracture risk in older women and men in the *Bone*

464 *Microarchitecture International Consortium.* *Lancet Diabetes Endocrinol.* 2019;7:34-43.

465. Chapurlat R, Bui M, Sornay-Rendu E, Seeman E et al. Deterioration of cortical and

466 trabecular microstructure identifies women with osteopenia or normal bone mineral density at

467 imminent and long-term risk for fragility fracture: a prospective study. *J Bone Miner Res*

468 2020; 35: 833-44.

46910. Leslie WD, Seeman E, Morin SN, Lix LM, Majumdar SR. The diagnostic threshold for  
470 osteoporosis impedes fracture prevention: A registry-based cohort study. *Bone* 2018;  
471 114:298-303.
47211. Colon-Emeric CS, Saag KG. Osteoporotic fractures in older adults. *Best Pract Res Clin*  
473 *Rheumatol.* 2006;20(4):695–706.
47412. Lyles K, Gold D, Shipp K, et al. Association of osteoporotic vertebral compression fractures  
475 with impaired functional status. *Am J Med.*1993;94:595–601.
47613. Diamond T, Champion B, Clark W. Management of acute osteoporotic vertebral fractures: a  
477 non-randomized trial comparing percutaneous vertebroplasty with conservative therapy. *Am J*  
478 *Med.* 2003; 114:257–65.
47914. Weiner S, Traub W (1992) Bone structure: from angstroms to microns. *FASEB J* 6:879–885
48015. Seeman E, Delmas PD. Bone quality – the material and structural basis of bone strength and  
481 fragility. *New Engl J Medicine.* 2006;354:2250-61.
48216. Muller R. Hierarchical microimaging of bone structure and function. *Nature Rev.*  
483 *Rheumatol.* 2009; 5:373-81.
48417. Ural A, Vashishth D. Hierarchical perspective of bone toughness-from molecules to fracture.  
485 *Int Mater Rev* 2014; 59:245–63
48618. Zimmermann EA, Schaible E, Bale H et al. Age-related changes in the plasticity and  
487 toughness of human cortical bone at multiple length scales. *Proc Natl Acad Sci USA* 2011;  
488 108:14416
48919. Akkus O, Polyakova-Akkus A, Adar F, Schaffler M. Aging of microstructural compartments  
490 in human compact bone. *J Bone Miner Res.* 2003;18:1012–1019
49120. Currey J. The mechanical consequences of variation in the mineral content of bone. *J*  
492 *Biomechanics.* 1969;2:1-11.

4921. Zebaze RM, Ghasem-Zadeh A, Bohte A, et al. Intracortical remodelling and porosity in the  
494 distal radius and post-mortem femurs of women: a cross-sectional study. *Lancet*.  
495 2010;375:1729–36.
4922. Schaffler MB, Burr DB. Stiffness of compact bone: effects of porosity and density. *J*  
497 *Biomech*. 1988;21:13–6
4923. Yeung SSY, Reijnierse EM, Pham VK et al J Cachexia, sarcopenia and muscle. Sarcopenia  
499 and its association with falls and fractures in older adults: A systematic review and meta-  
500 analysis. 2019; 10: 485-500.
5024. Lakhani P, Prater AB, Hutson RK, et al. Machine learning in radiology: applications beyond  
502 image interpretation. *J Am Coll Radiol*. 2018;15:350–9
5025. Padoia V, Caliva F, Kazakia G et al Augmenting osteoporosis imaging with machine learning.  
504 *Current osteoporosis reports* 2021; 19: 699-709
5026. King SH and Shin CS Application of machine learning in bone and mineral research.  
506 *Endocrine and metab*. 2021; 36:928-37
5027. Kong SH, Ahn D, Kim B, Srinivasan K et al. A novel fracture prediction model using  
508 machine learning in a community-based cohort. *JBMR® Plus*. 4 (3), e10337
5028. Sornay-Rendu E, Boutroy S, François Duboeuf F, Chapurlat RD. Bone microarchitecture  
510 assessed by HR-pQCT as predictor of fracture risk in postmenopausal women: the OFELY  
511 Study. *J Bone Miner Res*. 2017;32:1243–51.
5129. Arlot M, Sornay-Rendu E, Garnero P, Vey-Marty B, Delmas PD. Apparent pre- and  
513 postmenopausal bone loss evaluated by DXA at different skeletal sites in women: the OFELY  
514 cohort. *J Bone Miner Res*. 1997;12:883–90.
5130. Chapurlat R, Pialat JB, Merle B, Confavreux E, Duvert F, Fontanges E, et al. The QUALYOR  
516 (QUalite Osseuse LYon Orleans) study: a new cohort for non-invasive evaluation of bone  
517 quality in postmenopausal osteoporosis. Rationale and study design. *Arch Osteoporos*. Dec 27  
518 2017;13(1):2. Epub 2017/12/29.

5191. Biver E, Durosier-Izart C, van Rietbergen B et al. Evaluation of radius microstructure and  
520 areal bone mineral density improves fracture prediction in postmenopausal women. *J Bone*  
521 *Miner Res.* 2018;33:328–37.
5222. Laib A, Häuselmann HJ, Rügsegger P. In vivo high-resolution 3D-QCT of the human  
523 forearm. *Technol Health Care.* 1998;6: 329–37.
5243. Kanis JA, Johnell O, Oden A, Johansson H, McCloskey E. FRAX and the assessment of  
525 fracture probability in men and women from the UK. *Osteoporos Int.* 2008;19(4):385–97.
5264. Huang, G., Liu, Z., Van Der Maaten, L. and Weinberger, K.Q., 2017. Densely connected  
527 convolutional networks. In *Proceedings of the IEEE conference on computer vision and*  
528 *pattern recognition* (pp. 4700-8).
5295. Kingma, D.P. and Ba, J., 2014. Adam: A method for stochastic optimization. *arXiv preprint*  
530 *arXiv:1412.6980*.
5306. Paszke, A., Gross, S., Massa, F., Lerer, A., Bradbury, J., Chanan, G., Killeen, T., Lin, Z.,  
531 Gimelshein, N., Antiga, L. and Desmaison, A., 2019. Pytorch: An imperative style, high-  
532 performance deep learning library. *Advances in neural information processing systems*, 32,  
533 pp.8026-37.
5347. Selvaraju, R.R., Cogswell, M., Das, A., Vedantam, R., Parikh, D. and Batra, D., 2017. Grad-  
535 cam: Visual explanations from deep networks via gradient-based localization. In *Proceedings*  
536 *of the IEEE international conference on computer vision* (pp. 618-26).
5378. Pepe, M. S. 2003. *The Statistical Evaluation of Medical Tests for Classification and*  
538 *Prediction.* Oxford: Oxford University Press.
5399. Huettner, Frank; Sunder, Marco (2012): Axiomatic arguments for decomposing goodness of  
540 fit according to Shapley and Owen values. *Electronic Journal of Statistics* 6, 1239-50.
5410. Zebaze R, Atkinson E, Peng Y, et al Increased Cortical porosity and reduced trabecular  
542 density are not necessarily synonymous with bone loss and microstructural deterioration.  
543 *JBMR Plus* 2019;3(4): e10078-85

5451. Ghasem-Zadeh A, Bui M, Seeman E et al. Bone microarchitecture and estimated failure load  
546 are deteriorated whether patients with chronic kidney disease have normal bone mineral  
547 density, osteopenia or osteoporosis. *Bone* 2022; 154 116260
5482. O'Brien FJ, Taylor D, Clive Lee T. The effect of bone microstructure on the initiation and  
549 growth of microcracks. *J Orthop Res* 2005; 23:475–80
5503. Currey JD Effects of differences in mineralization on the mechanical properties of bone. *Phil*  
551 *Trans. Royal Soc.Lond.* 1984; 304:509-18.
5524. Yeni YN, Brown CU, Wang Z, Norman TL. The influence of bone morphology on fracture  
553 toughness of the human femur and tibia. *Bone* 1997;21:453-9.
5545. Yeni YN, Norman TL (2000) Calculation of porosity and osteonal cement line effects on the  
555 effective fracture toughness of cortical bone in longitudinal crack growth. *J Biomed Mater*  
556 *Res* 51:504–9
5576. Burr DB, Schaffler MB, Frederickson RG (1988) Composition of the cement line and its  
558 possible mechanical role as a local interface in human compact bone. *J Biomech* 21:939–94.
5597. Ascenzi A, Bonucci E (1967) The tensile properties of single osteons. *Anat Rec* 158:375–86
5608. Goldman HM, Bromage TG, Thomas CD, Clement JG (2003) Preferred collagen fiber  
561 orientation in the human mid-shaft femur. *Anat Rec A Discov Mol Cell Evol Biol* 2003;  
562 272:434–45
5639. Buehler MJ (2008) Nanomechanics of collagen fibrils under varying cross-link densities:  
564 atomistic and continuum studies. *J Mech Behav Biomed Mater* 1:59–67
5650. Tang SY, Vashishth D Non-enzymatic glycation alters microdamage formation in human  
566 cancellous bone. *Bone* 2010; 46:148–54
5671. Nyman JS, Roy A, Shen X, Acuna RL, Tyler JH, Wang X The influence of water removal on  
568 the strength and toughness of cortical bone. *J Biomech* 2006; 39:931–8
5692. Hernandez CJ, Gupta A, Keaveny TM (2006) A biomechanical analysis of the effects of  
570 resorption cavities on cancellous bone strength. *J Bone Miner Res* 2006; 21:1248–55

5753. Fantner GE, Hassenkam T, Kindt JH Sacrificial bonds and hidden length dissipate energy as

572 mineralized fibrils separate during bone fracture. Nat Mater 2005; 4:612–6

573

574

575

576

577

578

579

580

581

582

583

584

585

586

587

588

589

590

591

592

593

594

595

596

597  
598  
599  
600  
601

**Table 1.** Median and interquartile ranges (IQR) for Structural Fragility Score-Artificial Intelligence (SFS-AI), Fracture Risk Assessment score (FRAX) with bone mineral density (BMD) and femoral neck BMD in women remaining fracture-free and women having Any Fragility Fractures or Major Fragility Fractures during 5 years follow-up.

	Non-Fracture (N = 350)		All Fragility Fractures (54)		p-value	Major Fragility Fractures (N = 24)		p-value
	Median	IQR	Median	IQR		Median	IQR	
SFS-AI	0.45	0.10	0.51	0.08	<0.001	0.50	0.10	<0.001
FRAX with BMD	6.00	5.10	7.70	7.30	0.160	7.85	7.10	0.304
BMD	-1.64	0.88	-1.69	0.98	0.961	-1.77	0.75	0.292

p-values comparing women with and without incident fractures computed using robust regression adjusted for age and cohort.

602  
603  
604  
605  
606  
607  
608  
609  
610  
611  
612  
613  
614  
615  
616  
617  
618  
619  
620  
621  
622  
623  
624  
625  
626  
627  
628  
629  
630  
631  
632  
633  
634  
635  
636

637  
638  
639  
640  
641

**Table 2** Performance of the Structural Fragility Score-Artificial Intelligence (SFS-AI) using data in women of any age and women aged 65 years and over

		All women of any age				Women aged 65 and older			
		Any Fragility Fracture (N = 422)		Major Fragility Fracture (N = 383)		Any Fragility Fracture (N = 236)		Major Fragility Fracture (N = 208)	
		Est	95% CI	Est	95% CI	Est	95% CI	Est	95% CI
AUC	Unadjusted	0.78	(0.73, 0.84)	0.76	(0.67, 0.85)	0.78	(0.71, 0.85)	0.76	(0.63, 0.88)
	Adjusted	0.74	(0.69, 0.79)	0.73	(0.65, 0.83)	0.73	(0.67, 0.80)	0.73	(0.61, 0.84)
OR	Unadjusted	3.44	(2.47, 4.78)	2.96	(1.85, 4.76)	3.21	(2.13, 4.83)	2.82	(1.55, 5.14)
	Adjusted	2.67	(2.03, 3.51)	2.53	(1.68, 3.82)	2.64	(1.86, 3.75)	2.54	(1.49, 4.34)
Sensitivity		65.7%	(53.4%, 76.7%)	58.1%	(39.1%, 75.5%)	74.0%	(59.7%, 85.4%)	68.2%	(45.1%, 86.1%)
Specificity		77.3%	(72.5%, 81.5%)	77.3%	(72.5%, 81.5%)	71.0%	(63.9%, 77.4%)	71.0%	(63.9%, 77.4%)

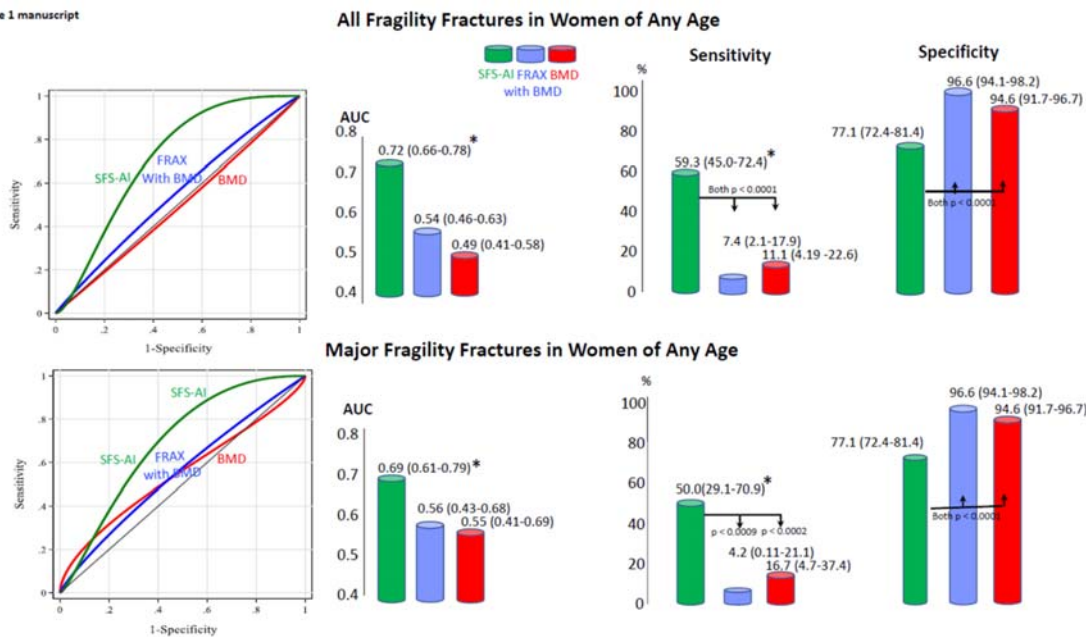
N= Sample size; Est = estimate; CI = confidence interval; Area under the curve (AUC) and odds ratios (OR) estimated with SFS-AI considered as continuous measurement and unadjusted and adjusted for age and cohort effect; Sensitivity and Specificity computed using clinical cut-off point of  $\geq 0.5$ .

642  
643  
644  
645  
646  
647  
648  
649  
650  
651  
652  
653  
654  
655  
656  
657  
658  
659  
660  
661  
662  
663  
664  
665  
666  
667  
668  
669  
670  
671  
672  
673  
674  
675  
676  
677  
678



679  
680  
681  
682  
683  
684  
685  
686  
687  
688

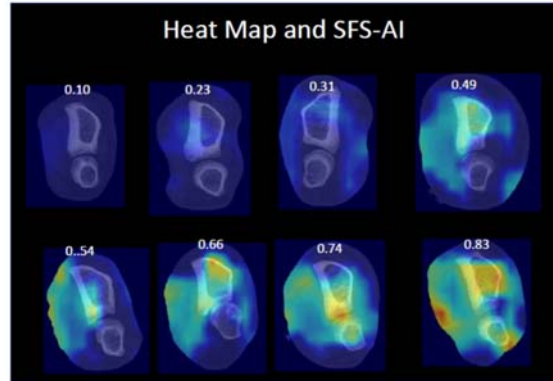
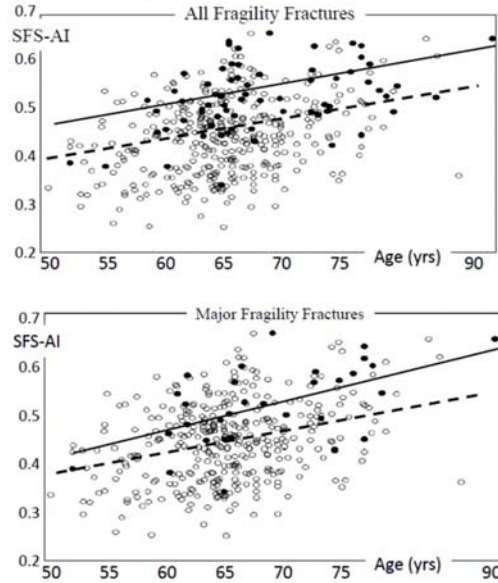
Figure 1 manuscript



689  
690  
691  
692  
693  
694  
695  
696  
697  
698  
699  
700  
701  
702  
703  
704  
705  
706  
707  
708  
709  
710  
711  
712  
713

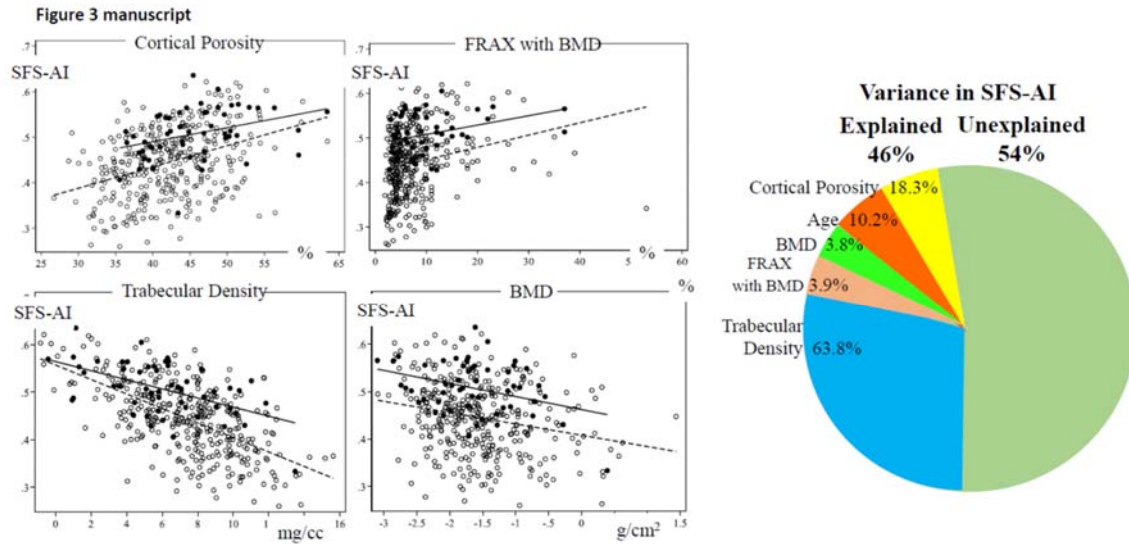
714  
715  
716  
717  
718  
719  
720  
721

Figure 2 manuscript



722  
723  
724  
725  
726  
727  
728  
729  
730  
731  
732  
733  
734  
735  
736  
737  
738  
739  
740  
741  
742  
743  
744  
745  
746  
747  
748

749  
750  
751  
752  
753  
754  
755  
756  
757



758  
759  
760  
761  
762  
763  
764  
765  
766  
767  
768  
769  
770  
771  
772  
773  
774  
775  
776  
777  
778  
779  
780  
781  
782  
783

784  
785  
786  
787  
788  
789  
790  
791  
792  
793  
794  
795  
796  
797  
798  
799  
800  
801  
802  
803  
804  
805  
806  
807  
808  
809  
810  
811  
812  
813  
814  
815  
816  
817  
818  
819  
820  
821  
822  
823  
824  
825  
826  
827  
828  
829  
830  
831  
832  
833  
834  
835

## Supplementary AI methods

**Deep Learning Network, training and the heat map** DenseNet used dense connection between layers and achieved efficacy in feature extraction. The first layer had a 110-dimension input instead of 3-dimension input in the original DenseNet.<sup>34</sup> We added a transition layer using 1\*1 convolution after the last denseblock of DenseNet to reduce the feature dimension from 1024 to 256 to extract a compact feature. A multi-task learning strategy was used to achieve more robust features. Extracted features were used to predict fractures during the ensuing 5-years, to predict the patient's age at the time of scanning and the duration of the fracture-free years of follow-up since scanning. The latter two tasks are included in the training to produce generalized feature representations powerful enough to be shared across different tasks.

We used a pretrained model as the initial model and 0.5 as the classification threshold for the training and validation. During training, cross-entropy loss was used as the fracture situation prediction loss, and used the mean squared error loss as the loss of age prediction and non-fracture year prediction. L1 regularization is performed on the weights of the classification layer to reduce overfitting. The model is optimized by ADAM optimizer using the four losses with weight 1 on the first three losses and weight 0.01 on the L1 regularization loss.<sup>35</sup> The learning rate is set as 5e-6 for the DenseNet backbone and 5e-5 for the other layers, including the transition layer and the three multi-learning branches. Pytorch is chosen to implement the model training and testing.<sup>36</sup> The Grad-CAM is utilized to generate the heatmap to represent the features that are extracted by the deep learning model.<sup>37</sup>

836  
837  
838  
839  
840  
841  
842  
843  
844  
845  
846  
847  
848  
849  
850  
851  
852  
853  
854  
855  
856  
857  
858  
859  
860  
861  
862  
863